Korean J. Chem. Eng., 32(9), 1864-1878 (2015)
DOI: 10.1007/s11814-015-0001-6

pISSN: 0256-1115
eISSN: 1975-7220

Two-stage batch sorber design and optimization of biosorption conditions by Taguchi methodology for the removal of acid red 25 onto magnetic biomass

Akeem Adeyemi Oladipo*,† and Mustafa Gazi**

*Department of Chemistry, Eastern Mediterranean University, Gazimagusa, TRNC via Mersin 10, Turkey
**Polymeric Materials Research Laboratory, Chemistry Department of Eastern, Mediterranean University, TRNC via Mersin 10, Turkey

(*Received 3 August 2014 • accepted 31 December 2014*)

Abstract−Biomagnetic material (MFC) was synthesized via simple co-precipitation and used as biosorbent for the removal of acid red 25 (AR25) under optimized conditions. The characteristics of MFC were studied using X-ray diffraction (XRD), Fourier transform infrared spectroscopy (FTIR), vibrating sample magnetometer (VSM), Boehm titration and scanning electron microscopy (SEM). Optimum removal of AR25 was achieved at pH=5.0. The equilibrium data were well described by the Sips and Freundlich models. Taguchi methodology was employed to optimize the biosorption experiments. 411.56 mg/g and 96.8% were obtained as the biosorption capacity and removal efficiency, respectively, at the optimum conditions of ionic strength (0.5 M), influent volume (300 L) and MFC dosage (4 g). The contact time for removal of 96% AR25 in two-stage batch system is 400.8 min which is lower than the single-stage treatment process (895 min).

Keywords: Biosorption Optimization, Ferula Communis, Taguchi Methodology, Two-stage Batch Sorber, Kinetics, Acidic Dyes

INTRODUCTION

Yearly, tons of heavily colored wastewater are released from various sources including leather, printing, textile, plastic and dye factories [1-6]. It is highly important to treat the colored hazardous effluents as they serve as threat to human beings and aquatic species. AR25 is one of the significant dyes that can initiate ecological problems due to its potential to reduce dissolved oxygen and sunlight penetration [7,8]. For these reasons, the removal of AR25 is mandatory for environmental protection and public health. Varying techniques with differing degree of success are available to treat polluted water. Most of these are capital intensive, and may result in the discharge of aromatic amines, formation of by-product and inability to efficiently treat diluted waste effluents [9,10].

Recently, biosorption technique has become an attractive alternative to traditional waste effluent treatment technologies due to the availability of biomass, low capital investment, ease of operation, insensitivity to toxic wastes and adequate removal of trace amount of hazardous substances from wastewater [11-13]. Consequently, various low-cost biosorbents have been investigated including *Ricinus communis*, seaweeds, coir pith, sawdust, rice husk *Pinus brutia* bark and eucalyptus bark [14-19]. Despite the biomass's attractive nature, the recovery and separation from the medium are restrictive factors limiting its industrial scale utilization.

However, these restrictions can be overcome via integration of magnetic recovery and separation methodologies to biosorption techniques [20]. The ease of separation with the use of a magnet, excellent mechanical characters, and improved biosorption ability are some of the features of magnetic biomaterial which serve as a promising biotechnological process. Hence, the search to prepare efficient smart biosorbents is still ongoing. *Ferula communis* (FC) is giant fennel that belongs to the family Apiaceae commonly found in Mediterranean region of Cyprus to central Asia. *Ferula communis* biomass could be a promising biosorbent due to its chemistry [21-23].

To the best of our knowledge, this is the first time $CuFe_2O_4$ has been integrated with FC to produce magnetic biosorbent to remove dye under optimization procedures. Conventional optimization procedures are cumbersome, involving high research costs and time consuming. However, the Taguchi approach is necessary to minimize the number of experiments and research costs.

Based on the above facts, the main objectives of the current research are to (1) prepare low-cost smart biosorbent (MFC) and examine its biosorption potential; (2) optimize the biosorption operational conditions including medium ionic strength, volume of influent, biosorbent dosage, etc., during the removal of AR25; (3) describe the optimized biosorption process using mathematical models; (4) discuss the biosorption mechanism of AR25 onto MFC and (5) optimize the contact time so as to reduce capital investment costs.

EXPERIMENTAL

1. Materials

F. communis plants were collected from Pergamos in North Cyprus, severally washed in tap water to remove dirt, and then in distilled water repeatedly. AR25 ($C_{20}H_{12}N_2Na_2O_7S_2$, FW=502.43, C.I.16050, λ_{max}=508 nm) was purchased from Merck (Germany). Other chem-

†To whom correspondence should be addressed.
E-mail: akeem.oladipo@emu.edu.tr

icals used were of analytical purity and obtained from Fluka (Switzerland).

2. Biosorbent Preparation

The washed biomass was dried at 60 °C for 12 h, crushed and sieved by laboratory standard sieve to produce less than 200 μm particle size biosorbent (FC). The magnetic biosorbents (MFC) were prepared by chemical co-precipitation of Cu^{2+} and Fe^{3+} ions by NaOH in the presence of FC followed by thermal treatment. The $CuFe_2O_4$ nanoparticles confer magnetic properties onto the raw FC.

Briefly, a known amount of FC was added to the solution of $Fe(NO_3)_3{\cdot}9H_2O$ (6.68 g) and $Cu(NO_3)_2{\cdot}3H_2O$ (2.0 g) in 120 ml of deionized water, and precipitated by 75 mmol of NaOH slowly until brownish-black precipitate was obtained. The homogenized mixture was stirred continuously at 90 °C for 4 h and later cooled to room temperature. The magnetic biosorbents obtained were separated by a magnet, then washed severally and kept in the oven overnight at 100 °C. MFC was ground in a laboratory mill, sieved and kept in a furnace at 600 °C for 6 h. The MFC was then cooled to room temperature for later use.

3. Adsorbate

500 mg/L stock solution of AR25 was prepared by dissolving carefully weighed amount of AR25 in doubly distilled water, and the desired working concentrations were obtained by dilution from the prepared stock solution. 0.1 M HCl and 0.1 M NaOH solutions were used for pH adjustment.

4. Biosorption Experiments

Certain amounts of MFC were transferred into 50 mL of varying concentrations of AR25 (50, 100, 150 and 200 mg/L) and agitated on a mechanical shaker at 200 rpm. 5 mL of samples was withdrawn from the reactor at a pre-set time interval and the concentration of AR25 was analyzed by a UV/VIS Spectrophotometer (Beijing, T80+). The effect of pH on AR25 biosorption was examined in the pH range of 1.0-10.0; the MFC was separated by external magnet and changed between 0.5 g and 3.0 g during the biosorption process. The ionic strength of the medium was varied from 0.5 to 2.0 M using NaCl solution. All the experiments were repeated three times for reproducibility tests and averages results were reported.

5. Taguchi Methodology and Data Evaluation

The Taguchi method is an easy and robust technique for optimizing biosorption parameters. Taguchi methodology was employed to examine how different bioprocess factors affect the variance and mean of biosorption efficiency and which variables contribute significantly to the process performance [24,25]. The Taguchi DOE employed in this work followed five sequential stages and was conducted by Reliasoft software (ver. 9.0, Reliasoft synthesis). The first step defines the different operational parameters to be optimized, including biosorbent dosage (m, g), ionic strength (i, M) and volume of influent (v, L) as presented in Table 1. The Taguchi orthogonal array L_9 (3^3) was designed for the selected operational parameters and their levels in the second and third steps based on the overall degree of freedom in the current study. The AR25 amount adsorbed onto MFC at equilibrium and at time t was calculated by the following equations:

$$q_e = \frac{(C_0 - C_e)V}{m} \tag{1}$$

$$q_t = \frac{(C_0 - C_t)V_0 - \sum_2^{i-1} C_{t_{i-1}} V}{m} \tag{2}$$

In the fourth step, the adsorption efficiency was predicted under optimum biosorption conditions. Finally, four confirmation experiments were performed at the optimized conditions to validate the Taguchi methodology.

6. Biosorption Isotherm

Isotherms analysis is significant for evaluating equilibrium data and describing the interactive influences between the biosorbent and the adsorbate [4,26-29]. Four widely used isothermal equations were applied to model the biosorption equilibrium data. The equations of the models, i.e., Freundlich (Eq. (3)), Sips (Eq. (4)), Langmuir (Eq. (5)) and Dubinin-Radushkevich (Eq. (6)), can be written as follows:

$$\ln q_e = \ln K_f + \frac{1}{n}\ln C_e \tag{3}$$

$$q_e = \frac{q_m K_s C_e^{1/n}}{1 + C_e^{1/n}} \tag{4}$$

$$\frac{1}{q_e} = \frac{1}{q_m K_L C_e} + \frac{1}{q_m} \tag{5}$$

$$\ln q_e = \ln q_m - \beta\varepsilon^2 \tag{6}$$

The mean biosorption energy, which can be computed from Eq. (7), provides information about the biosorption mechanism as chemical exchange (E>8 kJ/mol) or physical biosorption (E<8 kJ/mol) [30,31]. The mean biosorption energy is related to the activity coefficient and Polanyi potential according to Eq. (8), represented as follows;

$$E = \frac{1}{(2\beta)^{1/2}} \tag{7}$$

$$\varepsilon = RT\ln\left(1 + \frac{1}{C_e}\right) \tag{8}$$

7. Biosorption Kinetics

Four kinetic models were employed to evaluate the biosorption mechanism of AR25 onto MFC and to investigate the rate-limiting

Table 1. Designed L9 (33) orthogonal array for selected factors and assigned levels

Exp. no.	Factors and levels			Biosorption amount (q_e, mg/g)			SNR value
	A: i	B: v	C: m	q_1	q_2	Mean	
1	0.5 (1)	100 (1)	1 (1)	206.9	211.4	209.15	46.41
2	0.5 (1)	300 (2)	4 (2)	532.4	536.2	534.30	54.56
3	0.5 (1)	500 (3)	6 (3)	316.8	321.8	319.30	50.08
4	1.0 (2)	100 (1)	4 (2)	198.6	201.6	200.10	46.02
5	1.0 (2)	300 (2)	6 (3)	249.9	250.2	250.05	47.96
6	1.0 (2)	500 (3)	1 (1)	165.4	159.9	162.65	44.23
7	2.0 (3)	100 (1)	6 (3)	140.8	139.8	140.30	42.94
8	2.0 (3)	300 (2)	1 (1)	136.6	130.4	133.50	42.51
9	2.0 (3)	500 (3)	4 (2)	153.8	156.2	155.00	43.81

step. The linear forms of these equations can be expressed as follows:

Pseudo-first order kinetic model:

$$\ln(q_e - q) = \ln q_e - k_1 t \quad (9)$$

The initial biosorption rates $h_{0,1}$ (mg/g min) for AR25 onto MFC can be computed from the pseudo-first order model as follows:

$$h_{0,1} = k_1 q_e \quad (10)$$

Pseudo-second order kinetic model:

$$\frac{t}{q_t} = \frac{1}{kq_e^2} + \frac{t}{q_e} \quad (11)$$

The initial biosorption rates $h_{0,2}$ (mg/g min) for AR25 onto MFC can be computed from the pseudo-second order model as follows:

$$h_{0,2} = kq_e^2 \quad (12)$$

The Elovich model is one of the significant models applied to describe chemisorption, which predicts that the dye biosorption may involve valence forces via exchange or sharing of electrons between adsorbate and biosorbent. Elovich equation is as follows:

$$q_t = \alpha + \beta \ln t \quad (13)$$

The intra-particle diffusion model is necessary to identify the biosorption mechanism of AR25 onto MFC and can be expressed according to the following equation:

$$q_t = k_{it} t^{0.5} + C \quad (14)$$

Boyd's model was also applied to characterize the actual rate-controlling step involved during the biosorption process of AR25 onto MFC:

$$B_t = -0.4977 - \ln(1 - F) \quad (15)$$

The fraction of AR25 biosorbed at any time t, can be expressed as follows:

$$F = \frac{q_t}{q_0} \quad (16)$$

8. Two-stage Batch Sorber Design Analysis

Contact time optimization is undertaken here to be able to process more batches of effluents per day, resulting in lower treatment cost of polluted wastewater. The kinetic models can be integrated into mass balance equations to predict the design of multi-stage batch biosorption systems [32-34], and the basis of the model is discussed as follows.

The effluent to be treated contains V (L) of AR25 solution, and initial AR25 concentration C_0 (mg/L) entered the first treatment stage with biosorbent quantity M_1 (g) with q_0 (mg/g) loading of AR25 onto MFC. After attaining biosorption equilibrium and withdrawal of a certain amount, V (L) AR25 solution with concentration C_1 (mg/L) entered the second treatment stage. The AR25 concentration reduces from each stage to become C_i (mg/L) and the AR25 loading onto MFC increased from q_0 (mg/g) to q_i (mg/g). When fresh biosorbent was utilized, q_0=0 and the mass balance equation could be expressed as follows:

$$V(C_{i-1} - C_i) = M_i(q_{t,i} - q_0) = M_i q_{t,i} \quad (17)$$

Pseudo second-order equation is applied to describe the equilibrium in the two-stage biosorption process.

$$q_t = \frac{t}{1/kq_{e,i}^2 + t/q_{e,i}} \quad (18)$$

Combining Eqs. (17) and (18), the mass balance equation can be as expressed as follows:

$$C_{i-1} - C_i = \frac{M_i q_{t,i}}{V} = \frac{M_i kq_{e,i}^2 t}{V(1 + kq_{e,i} t)} \quad (19)$$

Total amount of AR25 removal can be evaluated analytically as follows:

$$\sum_{i=1}^{N}(C_{i-1} - C_i) = \sum_{i=1}^{N} \frac{M_i kq_{e,i}^2 t}{V(1 + kq_{e,i} t)} \quad (20)$$

The AR25 removal percentage in each biosorption stage, R_i, can be calculated from the following equation:

$$\sum_{i=1}^{N} R_i = \frac{100 M_i}{VC_0} \sum_{i=1}^{N} \frac{kq_{e,i}^2 t}{1 + kq_{e,i} t} \quad (21)$$

It is important for biosorber design to express q_e and k as a function of C_0.

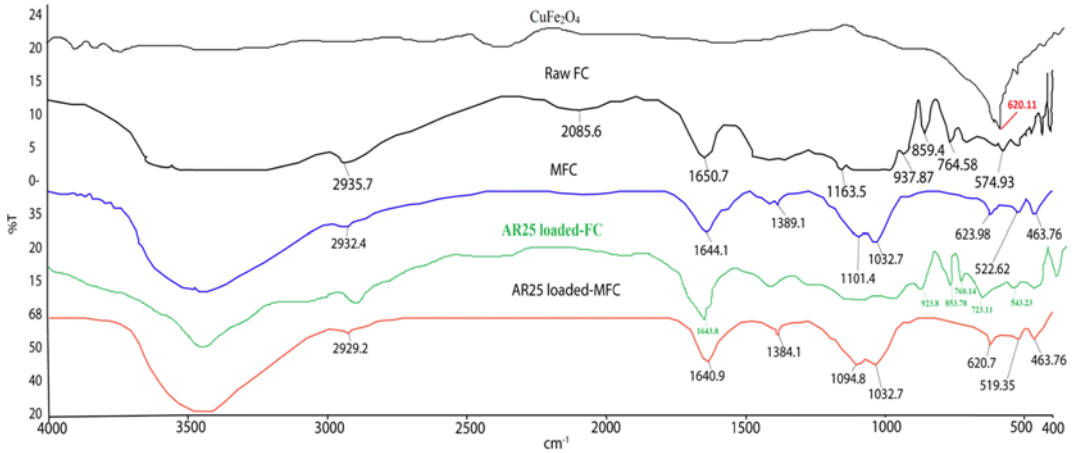

Fig. 1. FTIR spectra of raw Ferula communis, magnetic FC and AR25 loaded-MFC.

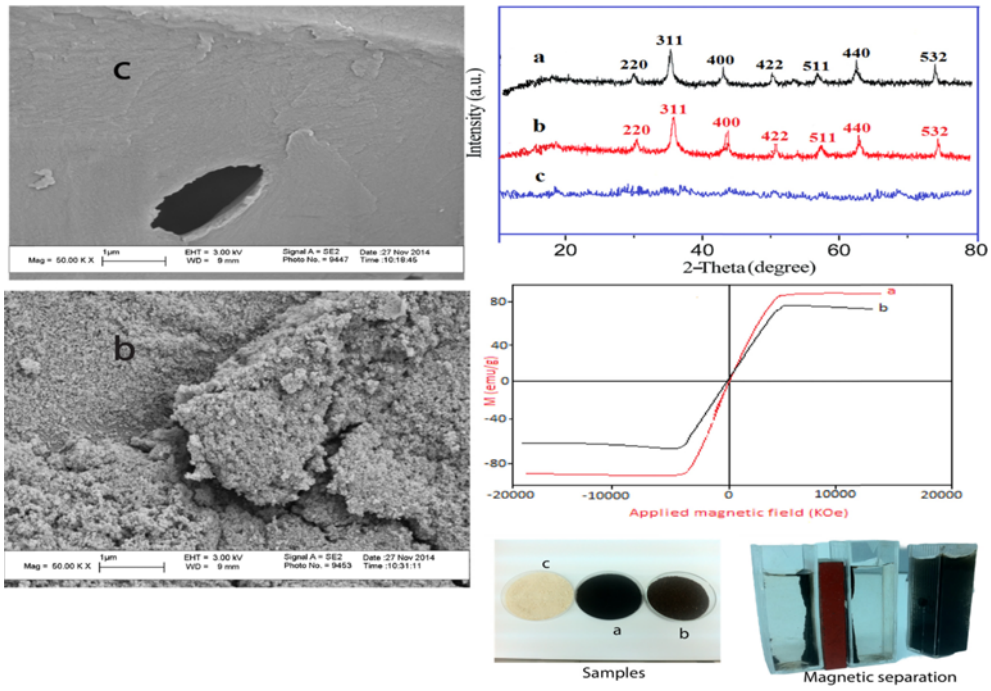

Fig. 2. SEM images, X-ray spectra, VSM curves, samples and separation process of (a) $CuFe_2O_4$ (b) MFC (c) FC.

RESULTS AND DISCUSSION

1. Characterization of Biosorbent

The FTIR spectra are useful to characterize the surface functional groups associated with MFC and those involved in biosorption of AR25 as shown in Fig. 1. The peak around 3,402 cm^{-1} in the raw FC is attributed to hydroxyl groups of lignin and cellulosic *F. communis* [21-23]. The peak C-O-C at 1,163.5 cm^{-1} also confirmed the cellulosic nature and the weak band at 2,935.7 cm^{-1} was attributed to the C-H stretch vibration bond in methylene groups. The peaks at 1,650.7, 1,644.1 and 1,640.9 cm^{-1} confirmed the presence of C=O groups in raw FC, MFC and AR25 loaded-MFC, respectively, and the strong IR band at 620.11 cm^{-1} in $CuFe_2O_4$ confirms CuFe-O vibration [35].

After modification with $CuFe_2O_4$, the obvious changes are strong broad peaks at 3,458.9 and slightly reduced peak at 1,644.1 cm^{-1} corresponding to OH and C=O groups, respectively. The disappearance of peaks at 937.87, 859.4 and 764.6 cm^{-1} and the strong IR band at 623.98 cm^{-1} confirms CuFe-O vibration. It can be concluded that $CuFe_2O_4$ nanoparticles have been successfully integrated with FC. There are no substantial changes in the AR25-FC and AR25-loaded MFC spectra compared to FC and MFC indicating that the mechanism of the biosorption may be physisorption [4,26].

The SEM micrographs of FC and MFC are presented in Fig. 2. As seen, FC exhibited smooth surface with wrinkles. MFC presents numerous particles homogeneously anchored onto the FC surface with size ranged from 20 to 100 nm, and average nanoparticles size of ≤50 nm. The introduction of $CuFe_2O_4$ particles led to a rough surface of MFC. The BET surface areas, $CuFe_2O_4$ content, pore volumes and magnetization measurement of samples are listed in Table 2.

The microporous volume and the surface area of MFC diminished slightly with an introduction of $CuFe_2O_4$ particles. However, the microstructure of MFC suggested that the pores of FC were

Table 2. BET surface area, magnetization and microstructure of FC, $CuFe_2O_4$ and MFC

FC	
Self-pH	6.20
pH_{zpc}	6.00
Moisture content (%)	8.98
BET surface area (m^2/g)	445
Specific saturation magnetization (emu/g)	0.0
Micro-pore volume (cm^3/g)	0.266
$CuFe_2O_4$ (wt%)	0.0
$CuFe_2O_4$	
BET surface area (m^2/g)	68.3
Specific saturation magnetization (emu/g)	89.75
Micro-pore volume (cm^3/g)	0.012
MFC	
pH_{zpc}	6.80
BET surface area (m^2/g)	393
Specific saturation magnetization (emu/g)	69.32
Micro-pore volume (cm^3/g)	0.196
$CuFe_2O_4$ (wt%)	1.1
Surface acidic functional groups (mmol/g)	
Phenolic	2.98
Lactonic	0.62
Carboxylic	1.45
Total acidic value	5.05

not all blocked by the presence of relatively small surface area and microporous volume of $CuFe_2O_4$ (68.3 m^2/g and 0.012 cm^3/g, respectively) [35,36]. The magnetic properties of the samples were investigated by a vibrating sample magnetometer (VSM) at room temperature. The plots of magnetization vs. magnetic field for $CuFe_2O_4$ and MFC are presented in Fig. 2. The magnetization curves indicate that both $CuFe_2O_4$ and MFC are super-paramagnetic with sufficient magnetization saturation values (89.75 emu/g and 69.32 emu/g, respectively). These magnetization values are sufficient enough to separate both samples from aqueous solution because saturation magnetization of 16.3 emu/g is adequate for magnetic separation using conventional magnet [35].

The synthesized samples were dispersed in water in small tubes, and external magnet with magnetic intensity of 0.8 T was placed in between the tubes to investigate the magnetic separability of the samples. As displayed in Fig. 2, the tubes containing dispersed samples were black and after a short period, clear water is seen and can be re-dispersed with slight shake. The results reveal that the synthesized materials could be separated easily from solutions with external magnet and could be potentially applied as magnetic biosorbent to remove pollutants.

The XRD patterns of FC, MFC and $CuFe_2O_4$ are illustrated in Fig. 2. No characteristic diffraction peaks were observed in the spectrum of FC, which indicates a long range disorder along with amorphous character, exist in FC [20]. The XRD patterns of MFC and $CuFe_2O_4$ show characteristics peaks at 30.2 (220), 36.5 (311), 43.5 (400), 53.7 (422), 58.5 (511), 65.1 (440) and 75.2 (532), which are consistent with the reflections indexed in (JCPDS 77-0010) and the most intense peak (311) confirmed the formation of spinel-type cubic structure of $CuFe_2O_4$ [37,38].

The pH_{zpc} of FC and MFC were determined as described elsewhere by pH drift method [4,26]. Twenty milligrams of the samples were mixed with known pH of 0.01 mol/L NaOH and N_2 gas was bubbled into the suspension for 3 h. The pH of the samples was adjusted between 1 and 12 under N_2 for 24 h. The final pH was determined and plotted against the initial pH, the pH_{zpc} was obtained when $pH_{final}=pH_{initial}$. As shown in Fig. 3(a), at $pH<pH_{zpc}$, the surface charge of MFC is net positive, and this can uptake the AR25 anions via electrostatic mechanism while the surface is a net negative at $pH>pH_{zpc}$. Boehm titration described in [39] was employed to quantify the oxygenated acidic surface on MFC and obtained results are presented in Table 2.

2. Effect of Solution pH

The solution pH is a significant factor affecting the removal of pollutants from aqueous media [40-42]. The pH dependence of AR25 biosorption onto MFC as shown in Fig. 3(b) indicates the highest biosorption removals of MFC were observed at solution pH=5.0 for all the investigated initial AR25 concentrations. Biosorption of anionic species is generally increased by increasing the H^+ concentration in the aqueous media. In this study, the effects of initial pH on percentage removal of AR25 dye solutions (100, 150 and 200 mg/L) onto MFC biosorbents were investigated within a pH range between 1 and 10.

AR25 biosorption removal percentage increases as the pH increases and this corroborated with the pH_{zpc} measurements. The percentage of AR25 removed increased markedly from 10.2, 13.5 and 18.5% at pH=2.0 for AR25 concentrations (100, 150 and 200 mg/L) to 28.7, 47.3 and 85. 2% removed at pH=5.0. The biosorption of AR25 occurred when the magnetic biosorbent presents a positive surface charge ($pH<pH_{zpc}$), while the dissolved AR25 dye is negatively charged in aqueous solutions, due to the presence of sulfonate groups leading to electrostatic interaction.

3. Effect of Biosorbent Dosage

The effect of MFC dosage on the biosorption of AR25 was examined and the results presented in Fig. 4(a). As shown, AR25 removal percentage increased from 21.5±0.5 to 91.4±0.6% when the bio-

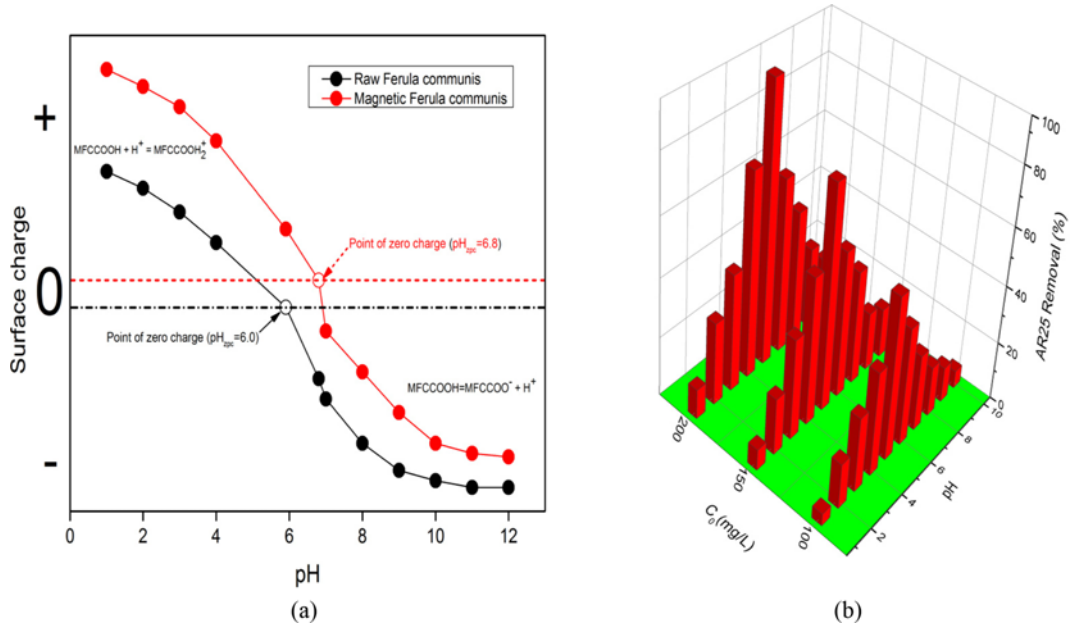

Fig. 3. (a) pH of zero charge for raw FC and MFC (b) effect of pH on AR25 biosorption at different concentrations.

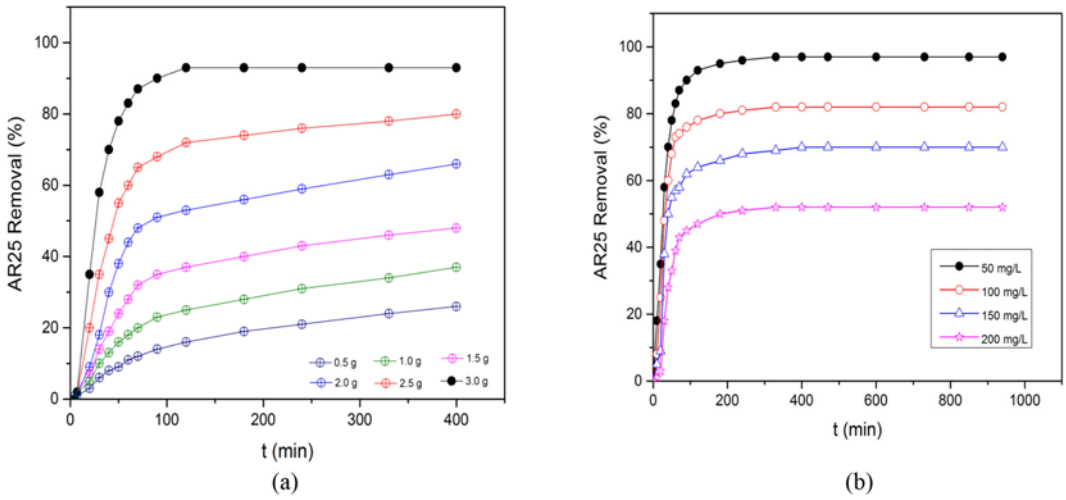

Fig. 4. (a) Effect of biosorbent dosage (b) effect of initial dye concentrations on AR25 biosorption onto MFC.

sorbent quantity was increased from 0.5 g to 3.0 g. Increase in biosorbent could increase the pollutant removal efficiency as more active surface sites were present for biosorption, and similar trends have been observed by other researchers [32-38]. In this context, increasing the biosorbent amount could be attributed to increase in the total surface functional groups on MFC leading to increased AR25 removal percentage.

4. Effect of Initial AR25 Concentration

Biosorption of AR25 at different initial concentrations as a function of contact time was investigated and the obtained results shown in Fig. 4(b). The removal of AR25 was rapid at the beginning and slowed down gradually until equilibrium was achieved. About 84.5% biosorption onto MFC was observed for initial AR25 concentration of 50 mg/L within 60 min, while the final AR25 removal was observed to reach 96.8% at 950 min.

The AR25 removal reached around 36.9% and 47.2% for initial concentration of 200 mg/L in 60 min and 950 min, respectively. The removal percent was observed to decrease with increasing initial AR25 concentration. It could be that, at lower AR25 concentrations, all adsorbate ions in the biosorption medium could interact with the MFC binding sites, leading to higher removal percentage. At higher AR25 concentrations, there is increased saturation of biosorption sites, resulting in decreased percentage uptake, and these observations fit well with the findings of other researchers [43-46].

5. Results of Taguchi Methodology

Taguchi model utilized statistical approach of performance known as SNR (signal to noise ratio) to evaluate the analysis data. The SNR performance features can be grouped as "smaller is better," "nominal is best" and "larger is better." The aim of this study was to improve the AR25 removal; therefore, larger is better (SNR) was chosen and expressed as follows:

$$SNR = -10\log\left(\frac{1}{n}\sum_{i=1}^{n}\frac{1}{y_i^2}\right) \quad (22)$$

Based on Taguchi orthogonal array, nine experiments were conducted and each replicated twice. The response data of mean and SNR for elucidating the influence of each factor at the three selected levels on AR25 removal is presented in Table 3. The graphical representation of the main effects for mean and SNR response for each parameter studied is shown in Fig. 5.

Table 3. Response date for SNR and means for larger is better category

Level	SNR factors			Means factors		
	A: i	B: v	C: m	A: i	B: v	C: m
1	50.35	45.12	44.38	354.25	183.18	168.43
2	46.07	48.34	48.13	204.27	305.95	296.47
3	43.08	46.04	46.99	142.93	212.32	236.55
Delta	7.26	3.22	3.75	211.32	122.77	128.04
Rank	1	3	2	1	3	2

Optimization of the influencing parameters is significant for maximizing the AR25 biosorption onto MFC. Most studies have not considered the interactive effects of ionic strength, influent volume and biosorbent dosage. In this study, the combined effects of the mentioned input parameters were investigated and data obtained fitted into Taguchi matrix so as to understand the interactive influences of these parameters on the response (biosorption),and this may generate attractive points to various researchers in the field.

As shown in Fig. 5, "larger is better" was adopted for maximizing the mentioned input parameters; the biosorption ability of MFC decreases rapidly with increasing ionic strength from 0.5 to 1.0 M, and further increase in the medium ionic strength to 2.0 M decreases the biosorption ability. This phenomenon could be explained theoretically: when the electrostatic forces between the adsorbate ions and biosorbent surface were attractive, as in our case, an increase in ionic strength would decrease the biosorption capacity [47-49].

As the volume of influent in the batch reactor increases from 100 to 300 L, the SNR and means increase too, but further increase to 500 L results in a decrease in biosorption ability of MFC and similar results were observed for biosorbent dosage as shown in

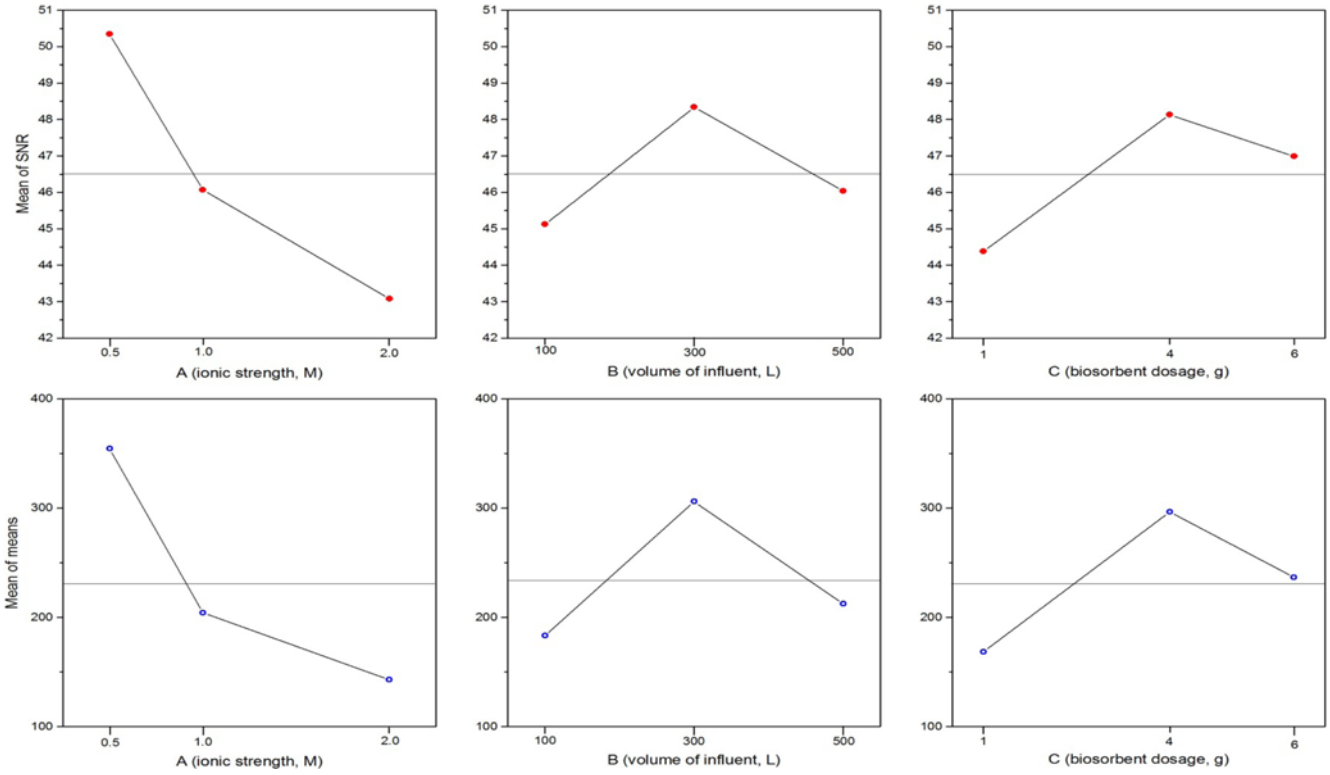

Fig. 5. Effect of operational factors on SNR and means of AR25 biosorption.

Table 4. Results of ANOVA for SNR and means for AR25 biosorption

Source	Sum of squares	DOF	Variance	*F*-ratio	Contribution (%)
SNR					
A: i	342.279	2	171.14	364.13	48.29
B: v	162.429	2	81.21	172.79	22.91
C: m	203.212	2	101.61	216.19	28.67
Error	0.948	2	0.47	------	0.13
Total	708.868	8	------	------	100
Means					
A: i	1824.201	2	912.11	16.25	65.08
B: v	348.111	2	174.06	3.10	12.42
C: m	518.424	2	259.21	4.62	18.50
Error	112.201	2	56.10	------	4.00
Total	2802.937	8	------	------	100

DOF, degree of freedom

Fig. 5. Increasing the SNR and means correspond to increasing the biosorption ability of MFC; therefore, the peak points in the response plots correspond to optimum biosorption condition [43,44,46]. Based on the SNR and means, the optimum conditions are A_1 (0.5 M), B_2 (300 L) and C_2 (4 g).

6. Analysis of Variance (ANOVA) Data

To examine systematically the relative significance of each factor on biosorption of AR25, analysis of variance was employed to the working results. The ANOVA data for the means and SNR are presented in Table 4, and the contribution percentage of each parameter is shown in Fig. 6(a)-(b). Based on the obtained data and the studied parameters, ionic strength was the most significant parameter on biosorption of AR25, followed by biosorbent dosage and volume of influent, respectively.

7. Efficiency Prediction and Confirmation Experiments

Efficiency prediction is a verification tests employed by Taguchi model to control the accuracy of experiments. The prediction of response (AR25 biosorption) based on the optimal combination of parameters obtained (A_1-B_2-C_2) can be computed theoretically using Eq. (23) as follows:

$$\eta_{opt}(\mathrm{AR25}) = m_t + \eta_{A1} - m_t + \eta_{B2} - m_t + \eta_{C2} - m_t = \eta_{A1} + \eta_{B2} + \eta_{C2} - 2m_t \quad (23)$$
$$= 50.35 + 48.34 + 46.99 - 2(46.50) = 52.68$$

The confidence interval (CI) for SNR of AR25 at the optimum conditions was computed using Eq. (24) and (25) as follows:

$$n_{eff} = \frac{N}{1 + \mathrm{DOF}_{opt}} = 1.00 \quad (24)$$

$$\mathrm{CI} = \pm\left(\frac{F_{0.05}(1, 2)V_e}{n_{eff}}\right)^{0.5} = \pm 0.732 \quad (25)$$

To evaluate the optimum biosorption efficiency of MFC, the expected data of SNR were transformed into the biosorbed amounts of AR25 using Eq. (22) and the predicted amount and confirmation results of AR25 optimization were tabulated in Table 5.

According to Taguchi model, a confirmation experiment is required to verify the predicted results, and if the observed results are within the corresponding predicted values, then the investi-

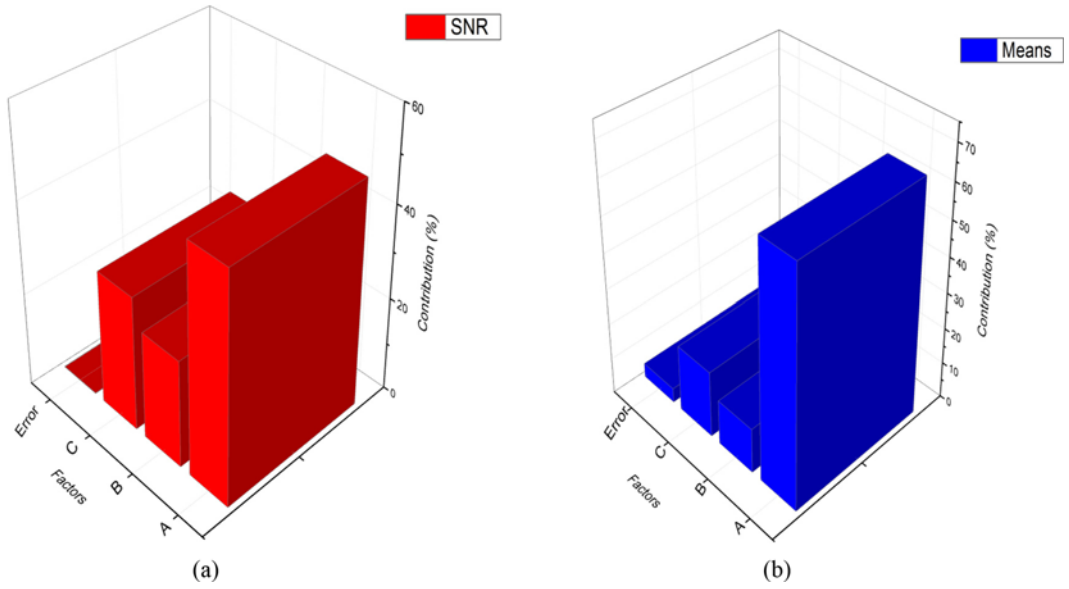

Fig. 6. Contribution of investigated parameter on AR25 biosorption for (a) SNR (b) means.

Table 5. Predicted value and results of confirmation experiment for AR25 biosorption

Dye	Predicted value			CI of SNR (dB)	Expected value range		
	Optimal combination	SNR (dB)	Biosorption (mg/g)		SNR (dB)	Biosorption (mg/g)	
AR25	A_1-B_2-C_2	52.68	430.52	±0.732	51.95-53.41	395.82-468.27	
Results of confirmation experiments							
N=4	Biosorption (mg/g)				Mean (mg/g)	S.D	R.S.D (%)
	408.22	431.64	406.22	400.26	411.56	13.79	3.35

Maximum adsorption capacity of some adsorbents for acid dyes.

Adsorbent	Adsorbate	Adsorption capacity (mg/g)	Kinetics	References
MFC	Acid red 25	411.56	Pseudo-second-order	This study
$MWCNT_S$	Acid red 18	166.67	Pseudo-second-order	[50]
Activated carbon	Acid red 97	82.08	Pseudo-second-order	[51]
Poplar wood	Acid red 18	3.90	Pseudo-second-order	[52]
Scallop shell	Acid Cyanine	500.00	Pseudo-second-order	[53]

MWCNTs: Multiwalled carbon nanotubes

gated optimum biosorption conditions can be regarded valid or vice versa [54,55]. Based on the results shown in Table 5, the mean amount of AR25 (411.56 mg/g) fits well with the predicted values and falls within the expected ranges; hence, the proposed optimum parameters combination and corresponding response in the Taguchi model employed here are valid.

8. Biosorption Equilibrium and Isotherm Modeling

Four widely utilized isotherms were employed to describe the biosorption process of AR25, and the relevant parameters of the investigated models were stated in Table 6. Based on the theoretical analyses, the determination of coefficients (R^2) of the linear form of Freundlich was much closer to unity (1.0) than other investigated models. Furthermore, the values of 1/n for all the investigated concentrations were lower than unity, which indicates that the surface of MFC is majorly made up of heterogeneous biosorption binding sites and high biosorption intensity.

Meanwhile, the Sips model was likewise applied, which is considered a combination of Freundlich and Langmuir models [13, 56,57]. Based on the tabulated results, the heterogeneity factor of Sips model, 1/n<1, indicated MFC possess heterogeneous binding surfaces. In this context, the Sips equation would reduce to Freundlich model since all the investigated concentrations showed 1/n<1 with considerable high R^2 values.

Furthermore, from the analysis of D-R model, the mean biosorption energy (E) could be computed according to Eqs. (6) and (7). The biosorption characters were described as chemical when E values were more than 8.0 kJ/mol but physical when E values ranged between 1.0 and 8.0 kJ/mol. Based on the tabulated data, the mean biosorption energy for AR25 were all below 8.0 kJ/mol with R^2 values all above 0.9. This showed AR25 biosorption behav-

Table 6. The isotherms parameters for AR25 biosorption onto MFC

Concentrations (mg/L)	50	100	150	200
Langmuir				
$q_{e,exp}$ (mg/g)	284.6	408.2	618.3	795.8
q_m (mg/g)	206.2	316.8	566.7	602.8
K_L (L/g)	32.99	49.64	39.59	54.60
R^2	0.902	0.897	0.887	0.913
Freundlich				
$q_{e,exp}$ (mg/g)	284.6	408.2	618.3	795.8
K_f (L/g)	171.3	208.4	275.9	349.5
n	3.653	3.989	4.081	5.682
R^2	0.996	0.998	0.997	0.999
Sips				
$q_{e,exp}$ (mg/g)	284.6	408.2	618.3	795.8
q_m (mg/g)	234.4	432.6	600.8	758.9
K_s (L/g)	0.063	0.089	0.126	0.144
n	2.566	2.896	3.476	3.896
R^2	0.992	0.988	0.969	0.959
Dubinin-Radushkevich				
E (kJ/mol)	6.480	6.961	7.022	7.353
R^2	0.991	0.976	0.994	0.962

Table 7. The kinetic parameters for AR25 biosorption onto MFC

Concentrations (mg/L)	50	100	150	200
Pseudo-first order				
$q_{e,exp}$ (mg/g)	234.6	396.9	598.6	793.6
$q_{e,cal}$ (mg/g)	79.6	132.9	324.8	529.8
k_1 (1/min)	0.00351	0.00279	0.00231	0.00175
$h_{0,1}$	0.279	0.371	0.750	0.927
R^2	0.921	0.942	0.968	0.972
Pseudo-second order				
$q_{e,exp}$ (mg/g)	234.6	396.9	598.6	793.6
$q_{e,cal}$ (mg/g)	207.9	399.6	588.0	771.9
k (g/mg min)	0.00392	0.00132	0.00071	0.00045
$h_{0,2}$	169.43	210.77	243.75	267.53
R^2	1.000	0.996	0.995	0.998
Elovich				
$q_{e,exp}$ (mg/g)	234.6	396.9	598.6	793.6
$q_{e,cal}$ (mg/g)	179.6	220.6	496.8	620.3
α (mg/g min)	189.5	209.9	482.6	602.3
β (g/mg)	65.9	103.6	121.3	113.9
R^2	0.986	0.983	0.936	0.929
Intraparticle diffusion				
k_{d1} (mg/gmin$^{-0.5}$)	1.032	1.548	1.862	1.921
k_{d2} (mg/gmin$^{-0.5}$)	1.875	1.694	1.882	1.939
C_1	8.246	8.896	10.207	11.398
C_2	6.934	8.909	9.364	9.596
R_1^2	0.986	0.993	0.991	0.989
R_2^2	0.879	0.902	0.996	0.992
Boyd diffusion				
$D_p \times 10^5$ (cm^2/s)	1.94	1.25	0.99	0.65
$k_s \times 100$ (1/min)	3.46	2.84	1.40	0.89
R^2	0.979	0.989	0.991	0.996

iors by MFC were physical and consistent with the FTIR analyses.

9. Biosorption Kinetic Modeling

Four kinetic models were employed to describe the biosorption rates and obtained results presented in Table 7. The corresponding graphical representations are shown in Figs. 7(a)-(b). The values of correlation coefficients for pseudo-first order kinetics are not high for all the investigated AR25 concentrations, and the estimated $q_{e,cal}$ calculated from the model equation differ markedly from the experimentally measured values. This shows that the biosorption process did not obey the pseudo-first order equation.

The values of the correlation coefficient (R^2) for the pseudo-second order were ≥0.995 for all AR25 concentrations investigated, and the biosorption capacities calculated by the model fit well to those determined experimentally. Therefore, pseudo-second order, which is based on the assumption of sharing of valence forces, was feasible to describe the biosorption behavior of AR25 onto MFC. Elovich constants were obtained from the intercept and slope of

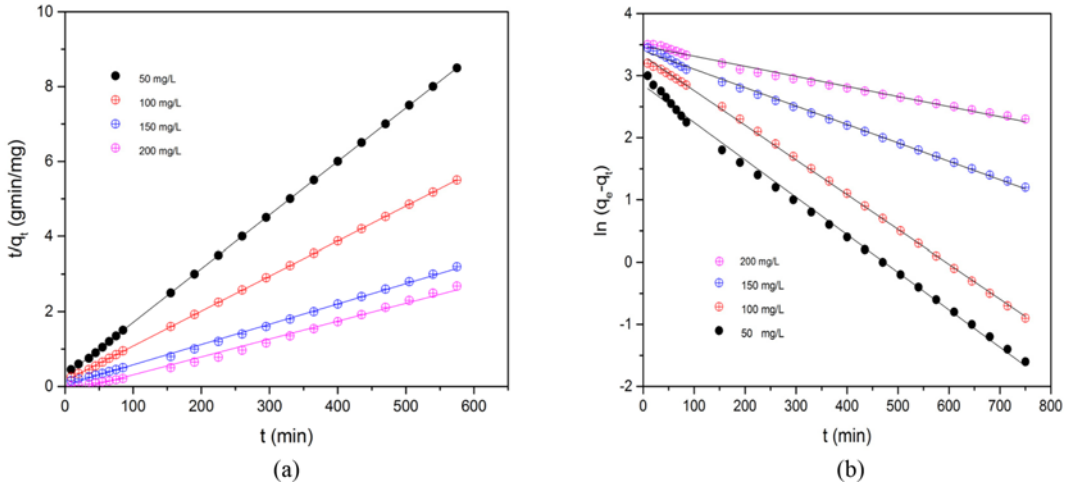

Fig. 7. Kinetic plots for AR25 biosorption: (a) pseudo-second order (b) pseudo-first order (T=25±0.5 °C; pH=5.0; dosage=4.0 g).

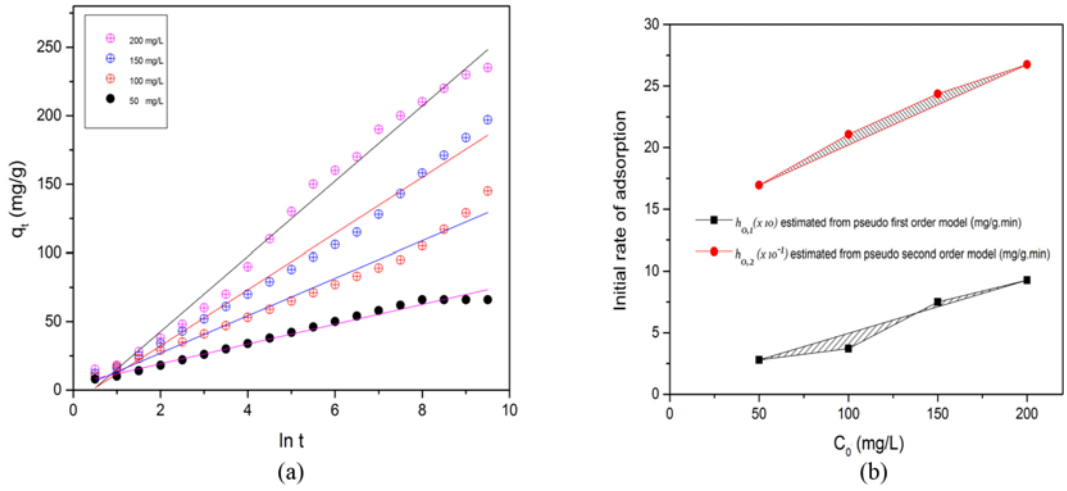

Fig. 8. Kinetic plots for AR25 biosorption: (a) Elovich (b) initial rates of biosorption (T=25±0.5 °C; pH=5.0; dosage=4.0 g).

the model plot as shown in Fig. 8(a). The correlation coefficient (R^2) from Elovich model ranged between 0.929 and 0.986, which were lower than those obtained from pseudo-second order equation.

Therefore, the kinetic fit follows the following order in this context: pseudo-second order>Elovich>pseudo-first order. The initial rates of AR25 biosorption were calculated using Eqs. (10) and (12) and the general trend observed as shown in Fig. 8(b) is an increase in the initial rate of biosorption with increasing AR25 initial concentration. As observed, the $h_{0,2}$ increases steadily with increasing initial concentration, unlike $h_{0,1}$, this further confirmed the estimation that pseudo-second order is more reliable to express the biosorption process of AR25 onto MFC.

10. Biosorption Mechanism

The overall adsorbate biosorption onto biosorbent surface may be characterized by several steps: film diffusion, surface diffusion, pore diffusion and biosorption into the pore cavity or combination of these steps [13,56]. Webber-Morris plot is based on the assumption that the dye uptake varies proportionally with $t^{0.5}$ rather than with contact time [57]. The plot of q_t versus $t^{0.5}$ should be linear if intraparticle is involved in the biosorption process, and the overall rate of biosorption will be governed by the slowest step, although the controlling step might be distributed between external and intraparticle transport mechanisms.

The intraparticle diffusion plot shown in Fig. 9(a), shows a multilinearity correlation, indicating that the three phases occur during the biosorption process of AR25. The first sharper stage (phase I) is transport of AR25 molecules from the bulk solution to the MFC external surface through film diffusion. The second stage (phase II) is the diffusion of the AR25 molecules from the boundary layer into the cavity of MFC, while the last stage (phase III) is the equilibrium portion where the AR25 molecules were biosorbed on the active sites within the pores of MFC and, intraparticle diffusion started to reduce due to lower AR25 concentration in the medium.

The obtained correlation coefficients for intraparticle diffusion (R^2=0.879-0.996), showed that intraparticle diffusion model was not only the rate governing step while other process might control the biosorption process. The linear portions of the intraparticle plots did not pass through the origin, indicating that the film diffusion controls the mass transfer rate of the initial linear segment while pore diffusion is not the overall step controlling at the

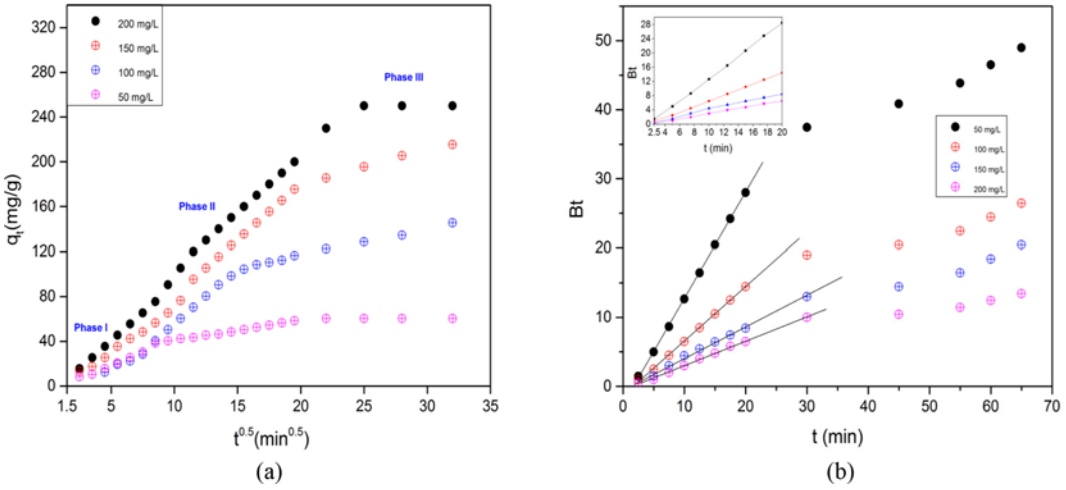

Fig. 9. (a) Intraparticle diffusion plots (b) Boyd plots for AR25 biosorption at different concentrations.

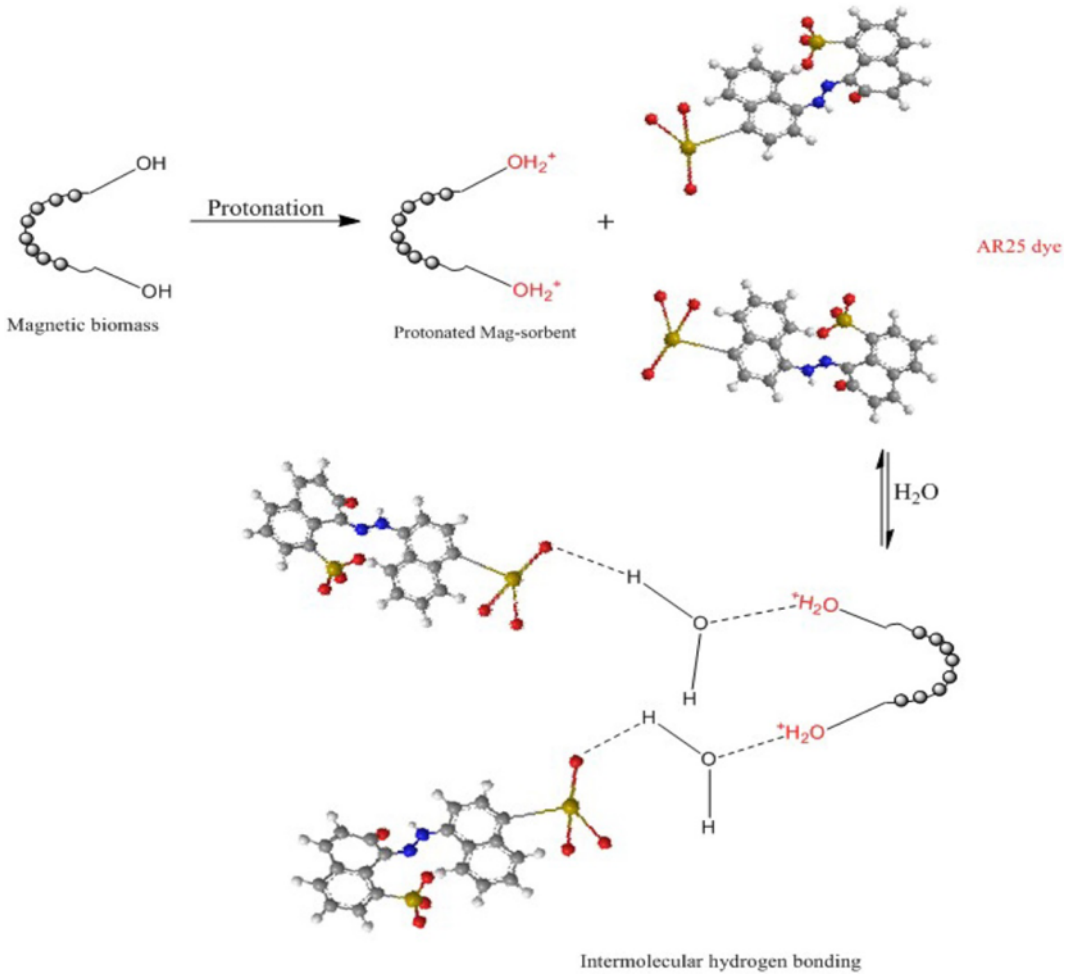

Fig. 10. Schematic representation of the biosorption process of AR25 and mechanism.

beginning of the biosorption. This observation could be elucidated further by the analysis of results from Boyd's equation [48-56].

Boyd's plot is used in predicting the actual rate controlling step. If a linear plot passing through the origin was obtained, then pore-diffusion governs the rate of mass transfer. A linear or non-linear Boyd's plot that does not pass the origin, is concluded to be film-diffusion controlled mechanism.

The first 65 min of Boyd's plot for AR25 biosorption is shown in Fig. 9(b); as seen, a short non-linear portion that does not pass the origin was observed, indicating that film-diffusion controlled the rate of biosorption at the first short stage. According to the data shown in Fig. 9(b) (inserted graph), the first portion was completed within about 20 min and was dominated by external mass transfer, facilitated by the existence of hydroxyl groups on the external surface of MFC.

As seen in Fig. 10, the H_2O molecules play a major role in AR25-MFC interactions where AR25 molecules interacted with its sulfonic groups through chains of H-bonds formed by H_2O molecules and the net positive external surface of MFC. The mean biosorption energy also confirmed that the biosorption mechanism was physical. The second stage completed within about 65 min could be characterized as intraparticle diffusion mechanism and, this stage was the rate-limiting step due to concentration gradient between the solution and the inner cavity of the biosorbent. Similar results were observed by other investigators [58,59].

11. Thermodynamic Parameters of Biosorption

Thermodynamic studies of biosorption process are important to conclude the spontaneity of the process. The data obtained experimentally at varying temperatures were used in calculating the thermodynamic parameters such as enthalpy change (ΔH), entropy change (ΔS) and Gibb's free energy change (ΔG).

The thermodynamic parameters were obtained from the slope and intercept of the plot of ln K_d versus 1/T as depicted in Eq. (26):

$$\ln K_d = \frac{\Delta S}{R} - \frac{\Delta H}{RT} \tag{26}$$

The negative values of ΔG signify the feasibility and spontaneous nature of the biosorption process. The decrease in ΔG values with increasing temperature indicated that the biosorption of AR25 was more spontaneous at higher temperature. Also, the data presented in Table 8 revealed the biosorption mechanism to be physical. Generally, the Gibb's free energy change for chemisorption ranges between −80 and −400 kJ/mol, but physisorption ranges between −20 and 0 kJ/mol [55,59]. The negative values of ΔH and positive values of

Table 8. Thermodynamic parameters for AR25 biosorption onto MFC

			Temperature (K)			
			298	308	318	328
AR25 (mg/L)	ΔH (kJ/mol)	ΔS (j/molK)	ΔG (kJ/mol)			
50	−5.320	40.535	−17.399	−17.805	−18.210	−18.615
100	−4.328	36.895	−15.322	−15.692	−16.061	−16.430
150	−3.546	29.895	−12.455	−12.753	−13.053	−13.351
200	−2.987	25.689	−10.633	−10.889	−11.147	−11.403

ΔS indicated an exothermic nature of biosorption and good affinity and increased randomness of AR25 towards MFC external surface, respectively.

12. Two-stage Batch Sorber Design Analysis

The application of time optimization model is employed in this study so as to reduce the treatment plant cumbersome factors and further reduce the plant capital investment [60,61]. The pseudo-second order kinetic plots were regressed to obtain expression for q_e and k values in terms of initial AR25 concentration as follows:

$$q_e = 5.06C_0^{0.949} \quad (27)$$

$$k = 1.75C_0^{-1.56} \quad (28)$$

For a two-stage countercurrent biosorption system, Eqs. (27) and (28) were inserted into Eq. (21) to determine AR25 biosorbed for a fixed removal percentage.

$$R_i = \frac{100M_i(1.75C_0^{-1.56})(5.06C_0^{0.949})^2 t}{VC_0[1+(1.75C_0^{-1.56})(5.06C_0^{0.949})t]} \quad (29)$$

The total AR25 biosorbed at any given initial concentration and the reaction contact time can be determined using the following expression:

$$\sum_{i=1}^{N} R_i = \frac{100M_i}{VC_0}\sum_{i=1}^{N}\frac{(1.75C_0^{-1.56})(5.06C_0^{0.949})^2 t}{[1+(1.75C_0^{-1.56})(5.06C_0^{0.949})t]} \quad (30)$$

For instance, 10 m^3 of a solution is to be treated, and 5 kg biosor-

Table 9. Minimum biosorption times to achieve various % AR25 removals for single and two-stage biosorption systems

	Two-stage				Single-stage
Dye removal (%)	System no.	Stage 1 (min)	Stage 2 (min)	Total time (min)	Contact time (min)
96 Removal	16	180	220.8	400.8	895
90 Removal	12	140	143.9	283.9	599
86 Removal	10	120	109.5	229.5	476
83 Removal	08	100	92.6	192.6	356
80 Removal	08	100	62.6	162.6	376

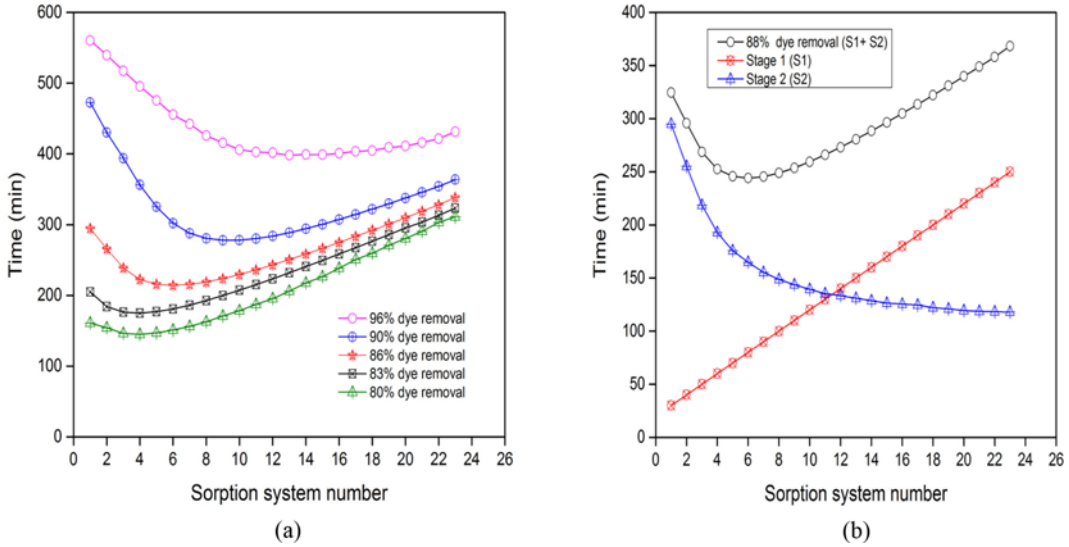

Fig. 11. (a) Minimum contact time for various percentage AR25 removals in a two-stage process (b) comparison of 88% AR25 removal time of each stage in two-stage process (T=25±0.5 °C; pH=5.0; dosage=4.0 g).

bent added to each of the two stages containing 150 mg/L AR25 in the first stage. Series of contact times from 30 min up to 600 min in 10 min increments have been specified in the first stage of the two-stage biosorption system for AR25 and expressed as follows:

$$t_1=30+(N-1)10 \text{ min} \quad (31)$$

In the first batch sorber, for instance, system 15 signifies that the first batch contact is 30 min+(15-1) 10 min=170 min. The total contact time T, to achieve a fixed total percent AR25 removal can be calculated as follows:

$$T=t_1+t_2 \quad (32)$$

Therefore, the total batch contact time can be computed as:

$$T=30+(N-1)10+t_2 \quad (33)$$

The minimum contact times for five various percentages AR25 removal are stated in Table 9 and the graphical representations for the stage 1+stage 2 are in Fig. 11(a). For 96% AR25 removal, the minimum contact time is 400.8 min as shown by system 16 with 180 min contact time for first stage and 220.8 min for second stage.

The times required by single stage process for same removal percentage are compared with two-stage process and given in Table 9. As shown, more time is required to achieve same AR25 removal as compared to two-stage process. The needed times for 80-96% AR25 removal in a single batch sorber increased 214-495 min.

Fig. 11(b) shows contact time and system number plot for 88% AR25 removal from 150 mg/L at 60% and 88% removal for stage 1 and stages 1+2, respectively. We assume stage 1 of the biosorption process has fixed contact times. For this investigation, series of contact times from 30 min up to 400 min in 15 min interval have been used, and the obtained data is specified in Fig. 11(b).

13. Reusability of the MFC without Regeneration

The magnetic biosorbent (MFC) was evaluated for its capability and efficiency without regeneration. The stability of the dye loaded-MFC was studied firstly in different pH environments. It was observed that AR25 would be detached from MFC-AR25 system at pH>6.8 due to competitions between the negative adsorbent surfaces and sulfonic groups of AR25. Therefore, MFC-AR25 was thermally treated at 600 °C to render the organic carbon inactive and improve the binding ability of the spent adsorbent for reuse, and similar method has been used elsewhere [55,62,63]. Ten consecutive tests were conducted using initial AR25 concentration of 150 mg/L at pH 5.0 and 4 g of MFC.

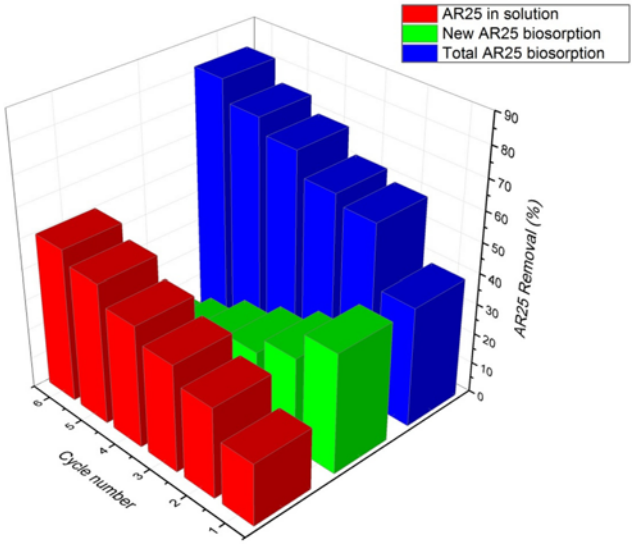

Fig. 12. Reuse of MFC without regeneration (pH: 5.0, AR25: 150 mg/L; T: 25 °C).

The biosorption study was completed in 2 h and the MFC was separated using magnet, dried for 24 h at room temperature and then reused in the second batch containing another 150 mg/L and so on. The obtained data as shown in Fig. 12 indicated that MFC is efficient to treat more polluted effluents without regeneration up to six cycles with decreasing loading biosorption capacity in each cycle.

CONCLUSION

Biomagnetic material for the removal of acidic dyes from aqueous media was prepared in this study.

- The biosorption of AR25 showed pH, ionic strength and dosage dependent but little variations with temperature. Taguchi model employed is effective for optimizing the treatment process.
- Pseudo-second order kinetics and intraparticle diffusion model played a significant role in the biosorption process.
- The application of two-stage biosorber model reduced the contact time by more than 50%. Overall, magnetic *F. communis* (MFC) is a high performance and effective biosorbent for the treatment of dye containing waters combined with its easy separation by magnet from aqueous media.

NOMENCLATURE

B_t : Boyd model constant
C_0 : initial AR25 concentration [mg/L]
C_e : AR25 concentration at equilibrium [mg/L]
C_t : AR25 concentration at time t [mg/L]
C : intraparticle diffusion model constant
CI : confidence interval
D_p : diffusion coefficient [cm^2/s]
E : mean biosorption energy [kJ/mol]
F : fraction of solute biosorbed at any time
FC : ferula communis biomass
k_1 : pseudo-first order kinetic rate constant [1/min]
k : pseudo-second order kinetic rate constant [g/mg min]
K_L : Langmuir biosorption constant [L/g]
K_f : Freundlich biosorption constant [L/g]
K_s : sips biosorption constant [L/g]
K_d : distribution coefficient
k_{id} : intraparticle rate constant [$mg/gmin^{0.5}$]
MFC : magnetic Ferula communis
M : mass of magnetic biosorbent [g]
m : mass of biosorbent (g)
m_t : total mean SNR of AR25
η_{A1} : mean SNR for A1 (parameter A and level 1)
n : Freundlich constant

η_{eff} : efficiency prediction
η_{opt} : predicted optimum SNR
q_e : amount of AR25 biosorbed onto biosorbent at equilibrium [mg/g]
q_t : amount of AR25 biosorbed onto biosorbent at time t [mg/g]
$q_{e,cal}$: amount of AR25 biosorbed onto biosorbent calculated at equilibrium [mg/g]
$q_{e,exp}$: amount of AR25 biosorbed onto biosorbent experimentally at equilibrium [mg/g]
q_m : maximum biosorption capacity for biosorbent [mg/g]
R : ideal gas constant [8.314 J/molK]
R_i : removal percentage [%]
R^2 : correlation coefficient
SNR : signal to noise ratio [dB]
T : absolute temperature [K]
t : time [min]
V : volume of solution [L]
V_e : variance
V_0 : volume of AR25 taken out every time [L]
ΔG : free energy change [J/mol]
ΔH : enthalpy change [J/mol]
ΔS : entropy change [J/mol K]

Greek Letters

β : mean free energy of biosorption per mole of the adsorbate [g/mg]
ε : polanyi potential
α : rate of chemisorption at zero coverage [mg/g min]

REFERENCES

1. A. A. Ahmad, B. H. Hameed and N. Aziz, *J. Hazard. Mater.*, **141**, 70 (2007).
2. B. H. Hameed and M. I. El-Khaiary, *J. Hazard. Mater.*, **159**, 574 (2008).
3. Y. S. Ho and G. McKay, *Can. J. Chem. Eng.*, **76**, 822 (1998).
4. A. A. Oladipo, M. Gazi and S. Sabar-Samandari, *J. Taiwan Inst. Chem. Eng.*, **45**, 653 (2014).
5. K. Rashid, S. K. Reddy, A. Al Shoaibi and C. Srinivasakannan, *Can. J. Chem. Eng.*, **9999**, 1 (2013).
6. H. Y. Zhu, Y. Q. Fu, R. Jiang, J. H. Jiang, L. Xiao, G. M. Zeng, S. L. Zhao and Y. Wang, *Chem. Eng. J.*, **173**, 494 (2011).
7. M. M. Ayad and A. A. El-Nasr, *J. Nanostruct. Chem.*, **3**, 3 (2012).
8. S. Jain and R. V. Jayaram, *Desalination*, **250**, 921 (2010).
9. S. Nethaji, A. Sivasamy, G. Thennarasu and S. Saravanan, *J. Hazard. Mater.*, **181**, 271 (2010).
10. P. Thamilarasu and K. Karunakaran, *Can. J. Chem. Eng.*, **91**, 9 (2013).
11. A. Thevannan, G. Hill and C. H. Niu, *Can. J. Chem. Eng.*, **89**, 176 (2011).
12. W. Zhang, H. Li, X. Kan, L. Dong, H. Yan, Z. Jiang, H. Yang, A. Li and R. Cheng, *Bioresour. Technol.*, **117**, 40 (2012).
13. S. Chowdhury, S. Chakraborty and P. D. Saha, *Environ. Sci. Pollut. Res.*, **20**, 1698 (2013).
14. K. Kadirvelu, K. Thamaraiselvi and C. Namasivayam, *Sep. Purif. Technol.*, **24**, 497 (2001).
15. A. E. Ofomaja and E. I. Unuabonah, *J. Taiwan Inst. Chem. Eng.*, **44**, 566 (2013).
16. D. Ozdes, A. Gundogdu, B. Kemer, C. Duran, M. Kucuk and M. Soylak, *Can. J. Chem. Eng.*, **92**, 139 (2014).
17. V. Sarin and K. K. Pant, *Bioresour. Technol.*, **97**, 15 (2006).
18. K. Vijayaraghavan, J. Jegan, K. Palanivelu and M. Velan, *Sep. Purif. Technol.*, **44**, 53 (2005).
19. J. X. Yu, L. Y. Wang, R. A. Chi, Y. F. Zhang, X. G. Xu and J. Guo, *Environ. Sci. Pollut. Res.*, **20**, 543 (2013).
20. F. Maggi, C. Cecchini, A. Cresci, M. M. Coman, B. Tirillini, G. Sagratini and P. Fabrizio, *Fitoterapia*, **80**, 68 (2009).
21. A. Marchi, G. Appendino, I. Pirisi, M. Ballero and M. C. Loi, *Biochem. System. Ecolog.*, **31**, 1397 (2003).
22. Y. Seki, M. Sarikanat, K. Sever and C. Durmuskahya, *Composites: Part B*, **44**, 517 (2013).
23. F. Deni, *Env. Prog. Sust. Energy*, **32**, 1129 (2013).
24. J. Liu, Y. Li and K. Li, *J. Env. Chem. Eng.*, **1**, 389 (2013).
25. V. K. Gupta, B. Gupta, A. Rastogi, A. Nayak and S. Agarwal, *J. Hazard. Mater.*, **186**, 891 (2011).
26. A. A. Oladipo and M. Gazi, *J. Water Process Eng.*, **2**, 43 (2014).
27. G. Ciobanu, M. Harja, L. Rusu, A. M. Mocanu and C. Luca, *Korean J. Chem. Eng.*, **31**, 1021 (2014).
28. H. Tang, W. Zhou and L. Zhang, *J. Hazard. Mater.*, **209-210**, 218 (2012).
29. N. M. Mahmoodi, B. Hayati, M. Arami and C. Lan, *Desalination*, **268**, 117 (2011).
30. W. Zhang, H. Yang, H. Li, Z. Jiang, L. Dong, X. Kan, H. Yang, A. Li and R. Cheng, *Chem. Eng. J.*, **168**, 1120 (2011).
31. S. Basha, Z. V. P. Murthy and B. Jha, *Chem. Eng. J.*, **147**, 226 (2009).
32. Y. S. Ho and C. C. Wang, *J. Hazard. Mater.*, **156**, 398 (2008).
33. M. Ozacar and I. A. Sengyl, *Biochem. Eng. J.*, **21**, 39 (2004).
34. S. T. Akar, Y. Y. Balk, O. Tuna and T. Akar, *Carbohydr. Polym.*, **94**, 400 (2013).
35. Y. Liu, M. Chen and Y. Hao, *Chem. Eng. J.*, **218**, 46 (2013).
36. L. Shao, Z. Ren, G. Zhang and L. Chen, *Mat. Chem. Phys.*, **135**, 16 (2012).
37. G. Zhang, J. Qu, H. Liu, A. T. Cooper and R. Wu, *Chemosphere*, **68**, 1058 (2007).
38. Y. J. Tu, C. F. You, C. K. Chang, T. S. Chan and S. H. Li, *Chem. Eng. J.*, **244**, 343 (2014).
39. A. A. Oladipo and M. Gazi, *J. Taiwan Inst. Chem. Eng.*, (2014), DOI:10.1016/j.jtice.2014.09.027.
40. T. Akar, Y. Y. Balk, O. Tuna and S. T. Akar, *Ecolog. Eng.*, **61**, 251 (2013).
41. M. F. Elkady, A. M. Ibrahim and M. M. Abd El-Latif, *Desalination*, **278**, 412 (2011).
42. M. S. Chiou and H. Y. Li, *Chemosphere*, **50**, 1095 (2003).
43. G. Crini and P. M. Badot, *Prog. Polym. Sci.*, **33**, 399 (2008).
44. M. Makeswari and T. Santhi, *J. Chem.*, **2013**, 12 (2012).
45. A. E. Ofomaja, *Biochem. Eng.*, **40**, 8 (2008).
46. G. Alberghina, R. Bianchini, M. Fichera and S. Fisichella, *Dyes Pigm.*, **46**, 129 (2000).
47. Y. S. Al-Degs, M. I. El-Barghouthi, A. H. El-Sheikh and G. M. Walker, *Dyes Pigm.*, **77**, 16 (2008).
48. Q. Li, Q. Y. Yue, Y. Su, B. Y. Gao and H. J. Sun, *Chem. Eng. J.*, **158**, 489 (2010).

49. K. Y. Foo and B. H. Hameed, *Chem. Eng. J.*, **156**, 2 (2010).
50. M. Shirmardi, A. Mesdaghinia, A. H. Mahvi, S. Nasseri and R. Nabizadeh, *J. Chem.*, **9**, 2371 (2012).
51. V. Gomez, M. S. Larrechi and M. P. Callao, *Chemosphere*, **69**, 1151 (2007).
52. R. Shokoohi, V. Vatanpoor, M. Zarrabi and A. Vatani, *J. Chem.*, **7**, 65 (2010).
53. M. S. Siboni, A. Khataee, F. Vafaei and S. W. Joo, *Korean J. Chem. Eng.*, **31**, 1451 (2014).
54. A. A. Oladipo and M. Gazi, *Toxicol. Env. Chem.*, (2014), DOI: 10.1080/02772248.2014.989854.
55. A. A. Oladipo and M. Gazi, *J. Water Process Eng.*, (2014), DOI: 10.1016/j.jwpe.2014.12.002.
56. R. Sips, *J. Chem. Phys.*, **16**, 490 (1948).
57. A. Mittal, *J. Hazard. Mater.*, **B133**, 196 (2006).
58. I. A. W. Tan, A. L. Ahmad and B. H. Hameed, *Chem. Eng. J.*, **137**, 462 (2008).
59. J. Y. Farah and N. S. El-Gendy, *Turkish J. Eng. Env. Sci.*, **37**, 146 (2013).
60. A. E. Ofomaja and E. I. Unuabonah, *Carbohydr. Polym.*, **83**, 1192 (2011).
61. V. Vadivelan and V. K. Kumar, *J. Colloid Interface Sci.*, **286**, 90 (2005).
62. W. Zhang, H. Yan, H. Li, Z. Jiang, L. Dong, X. Kan, H. Yang, A. Li and R. Cheng, *Chem. Eng. J.*, **168**, 1120 (2011).
63. W. Zhang, L. Dong, H. Yan, H. Li, Z. Jiang, X. Kan, H. Yang, A. Li and R. Cheng, *Chem. Eng. J.*, **173**, 429 (2011).